# The diffusion of fast ions in Ohmic TFTR discharges

W. W. Heidbrink,[a] Cris W. Barnes,[b] G. W. Hammett, Y. Kusama,[c] S. D. Scott, M. C. Zarnstorff, L. C. Johnson, D. McCune, S. S. Medley, H. K. Park, A. L. Roquemore, J. D. Strachan, and G. Taylor
*Plasma Physics Laboratory, Princeton University, Princeton, New Jersey 08543*

(Received 10 June 1991; accepted 19 July 1991)

Short duration (20 msec) neutral deuterium beams are injected into the TFTR tokamak [*Plasma Physics and Controlled Nuclear Fusion Research 1986* (IAEA, Vienna, 1987), Vol. I, p. 51]. The subsequent confinement, thermalization, and diffusion of the beam ions are studied with multichannel neutron and charge exchange diagnostics. The central fast-ion diffusion ($<0.05$ m$^2$/sec) is an order of magnitude smaller than typical thermal transport coefficients.

## I. INTRODUCTION

Two requirements for an ignited D–T fusion reactor are sufficient energy confinement of the thermal plasma and confinement of fusion-product alphas while they thermalize. Measurements of the diffusion of ions injected by neutral beams relate to both thermal confinement and alpha confinement. First, experimental thermal transport coefficients are generally inferred by *assuming* that the energetic ions that heat the plasma undergo no diffusion during thermalization. If this assumption has been incorrect, the inferred ion and electron thermal diffusivity profiles are erroneous, with consequent implications for theories of tokamak transport. Second, comparisons of fast-ion diffusion with thermal diffusion are useful in assessing the mechanisms responsible for anomalous thermal transport. Finally, beam-ion diffusion is relevant to fusion-product diffusion, because both beam ions and fusion products are characterized by gyroradii $\rho_f$ that are large compared to the thermal gyroradius $\rho_i$.

Although neoclassical fast-ion behavior in tokamaks is widely assumed, the experimental evidence supporting this assumption is scanty. Classical thermalization of beam ions was verified to 25% accuracy on DIII-D,[1] but radial transport was not studied. Measurements of ripple-trapped beam ions in TFR suggested some anomalous transport,[2] as did charge-exchange measurements on ISX-B.[3] Many other experiments found behavior roughly consistent with neoclassical transport, but the only quantitative bound on *central* beam-ion transport in the literature[4] is $D \lesssim 0.5$ m$^2$/sec. The most accurate previous study of beam-ion transport[5] established that the inward diffusion of a ring of toroidally "passing" beam ions in the outer region of TFTR[6] ($r > 0.35$ m) was smaller than 0.05 m$^2$/sec; however, this study did not address radial transport from the plasma center (where fast ions are generally created). In this paper, the bound on central beam-ion transport is lowered an order of magnitude to $D \lesssim 0.05$ m$^2$/sec, establishing for the first time that the central transport is comparable to neoclassical predictions.

## II. EXPERIMENT

The experimental technique is an extension of the short beam pulse experiments developed on Doublet III and DIII-D.[1] The basic idea of the experiment is to create a known beam-ion distribution and then observe its evolution in a well-diagnosed background plasma. Short ($\sim 20$ msec), intense ($\lesssim 20$ MW) pulses of deuterium neutral beams (83–96 kV) are injected into the steady-state portion of Ohmically heated, deuterium TFTR plasmas. The ions are injected with roughly equal amounts parallel and antiparallel to the plasma current at angles that have a minimum major radius between $R_{tan} = 1.73$ and 2.32 m. Since the beam pulse is short compared to the beam-ion deceleration time[7] ($\nu_E^{-1} \sim 420$ msec), the velocity distribution of the beam ions at the end of the pulse is essentially that of the injected neutrals, i.e., $\sim 48\%$ (by particle fraction) at 83–96 kV, $\sim 28\%$ at 42–48 kV, and $\sim 25\%$ at 28–32 kV. The initial spatial distribution of the beam is checked by comparing measurements of the neutron emission with calculations of the expected deposition profile. As expected, the deposition peaks strongly on axis (Fig. 1). The electron temperature is measured with electron cyclotron emission diagnostics[8] and the electron density is measured by inversion of ten-channel interferometer data;[9] both diagnostics have been compared extensively with Thomson scattering measurements[10] and have an absolute error of $\lesssim 10\%$. The plasma effective charge $Z_{eff}$ and deuterium density are inferred from tangential profiles of the visible bremsstrahlung emission.[11] Following the beam pulse, the central electron temperature decreases slightly ($\sim 7\%$), the line-average electron density increases by $\sim 15\%$, the central $Z_{eff}$ varies less than 5%, and the ion temperature and total pressure approximately double. Thus, the 100–250 kJ beam pulse constitutes a relatively minor perturbation to the electrons but a major perturbation to the ions. For all but one of the seven conditions studied, the calculated neutron source strength at the end of the beam pulse agrees to within 15% with the measured neutron emission (absolutely calibrated to $\pm 13\%$),[12] confirming that

[a] Permanent address: Department of Physics, University of California, Irvine, California 92717.
[b] Permanent address: Los Alamos National Laboratory, Los Alamos, New Mexico 87545.
[c] Permanent address: Naka-machi, Naka-gun, Ibaraki-ken 311-01, Japan.

 0899-8221/91/113167-04$02.00  

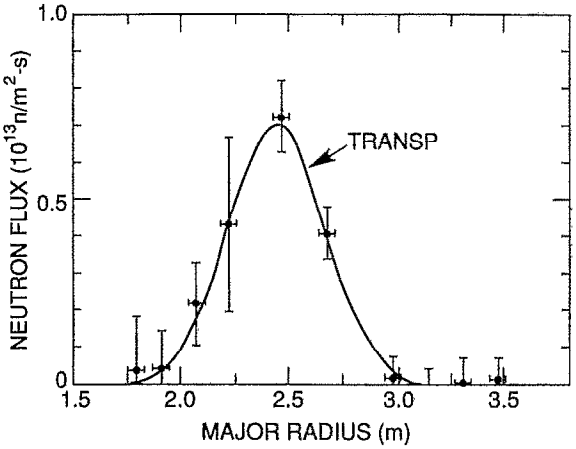


FIG. 1. Profile of the line-integrated 2.5 MeV neutron flux measured by the multichannel neutron collimator[13] for the 32 msec immediately following the beam pulse. Twenty-four similar pulses are added to improve counting statistics. The profile agrees well with the profile computed by the TRANSP code[17] for a single representative pulse.

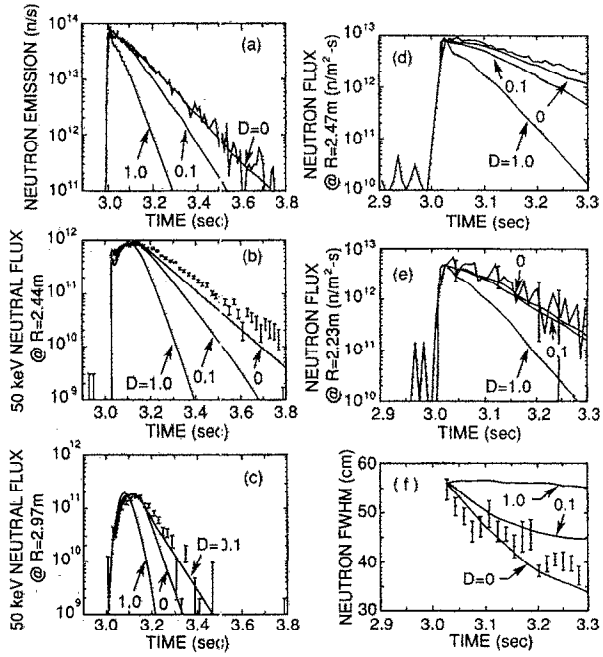


FIG. 2. Time evolution of the neutron and charge-exchange signals following a beam pulse at 3.0 sec in a discharge with $R = 2.42$ m, $a = 0.77$ m, $B_T = 4.1$ T, $I_p = 0.8$ MA, $\bar{n}_e = 0.8 \times 10^{19}$ m$^{-3}$, $T_e(0) = 3.9$ keV, and $Z_{\text{eff}} = 3.9$. The TRANSP Fokker–Planck predictions (normalized to the initial value) for various values of $D$ (in m$^2$/sec) are also shown. (a) Total neutron source strength. (b) On-axis 50 keV neutral flux. Seven similar pulses are summed to improve counting statistics (error bars). (c) Off-axis 50 keV neutral flux. Seven similar pulses are summed. (d) Central neutron flux. Twenty-four pulses are summed. (e) Off-axis neutron flux. Twenty-four pulses are summed. The error bars indicate typical errors, which become large late in time because the scattered signal becomes dominant. (f) Full width at half-maximum of a Gaussian fit to the neutron profile.[14] Twenty-four pulses are summed.

the initial beam and plasma characteristics are correctly measured and modeled.

The subsequent evolution of the beam population is inferred from neutron and charge-exchange measurements. The total 2.5 MeV neutron emission is measured by a set of fission detectors.[12] Calculations indicate that the signal is 60% beam–target reactions and 40% beam–beam reactions for the conditions of Fig. 1. The profile of the neutron emission is measured by ten vertically viewing, collimated neutron detectors.[13] The steep radial profile (Fig. 1) requires that multiple pulses (1–3 per shot) over many shots (4–10) are added to improve counting statistics in the outer channels. The dominant uncertainty in the neutron profile is associated with neutrons that backscatter off of machine components into neighboring channels. Specially formed, small minor radius plasmas are used to determine the scattering correction to the measured signals.[14] After corrections for scattering, the integral of the neutron profile agrees (within 20% uncertainty) with the measurements of the total neutron emission.[15] The third diagnostic system is a pair of vertically viewing $E \| B$ neutral-particle analyzers located at $R = 2.44$ and 2.97 m.[16] The contribution of scattered light is measured by three anodes above the injection energy and subtracted from the measured signals to obtain the actual neutral flux. Passive charge exchange is employed so that the measured chord-integrated signal is more heavily weighted toward the plasma edge than the neutron measurements, which are strongly weighted to the plasma core. A major difference between the charge-exchange and neutron diagnostics is that the charge-exchange diagnostics measure only banana-trapped ions, while the neutron signals are dominated by the toroidally circulating ion population.

The response of these diagnostics to a beam pulse at 3.0 sec is shown in Fig. 2. Since the fusion cross section decreases with decreasing energy, the neutron source strength falls as the beam ions decelerate [Fig. 2(a)]. The charge-exchange signal at 50 keV (just above the beam half-energy) first increases, then decreases as full-energy ions decelerate through 50 keV [Figs. 2(b) and 2(c)]. The collimated neutron signals from the plasma center [Fig. 2(d)] and ~0.20 m inboard from the magnetic axis [Fig. 2(e)] also decay as the beam ions decelerate. Since the beam ions in the center of the plasma take longer to decelerate than off-axis beam ions, the width of the neutron profile contracts with time [Fig. 2(f)]. For comparison, the fast-ion distribution is nearly isotropic (i.e., $p_\perp^{\text{fast}} \simeq 0.9 p_\parallel^{\text{fast}}$) 300 msec after the beam pulse.

The expected behavior of the signals for various diffusion coefficients is calculated using the TRANSP[17] code. Experimental inputs to the code include the neutral beam parameters, the electron temperature and density, the visible bremsstrahlung signal, and magnetics data (for the plasma shape). With these experimental inputs, the code calculates beam deposition, deceleration, and pitch-angle scattering using the classical formulas (with a typical accuracy of $\pm 9\%$ in the slowing-down time due to the experimental uncertainties). The evolution of the beam distribution can be calculated by a Monte Carlo technique[17] or by a Fokker–Planck treatment.[18] The two techniques typically agree to

within 5% for calculations of the rate of decay of the neutron source strength. An empirical, spatially constant, beam diffusion coefficient may be incorporated in the calculations. After the beam distribution is calculated, the expected signals are computed for the various diagnostics. In the calculation of the charge-exchange signals, the neutral density is assumed poloidally and toroidally symmetric with a time-evolving magnitude that is consistent with the measured poloidally averaged $D_\alpha$ signal.[19] The edge $D_\alpha$ signals at various poloidal positions increase from 20% to 80% in response to a beam pulse, but the shape of the neutral profile is not calculated to change while the beam population evolves. Since the charge-exchange sight lines do not intersect the path of the neutral beams and the limiter is the toroidally symmetric inner wall, the assumption of toroidal symmetry is reasonable for these plasmas.

The predicted decay in total neutron emission and central neutron emission becomes faster as the diffusion coefficient $D$ increases [Figs. 2(a) and 2(d)], because the fast-ion population, initially strongly peaked at the center, diffuses outward in minor radius to regions of shorter thermalization time. Off axis, the predicted decay rate only becomes shorter for large values of $D$, since transport from the plasma center balances outward losses [Fig. 2(e)]. The contraction of the neutron profile is retarded by diffusion, since central beam ions move radially outward [Fig. 2(f)]. For the central charge-exchange signal, the dependence on $D$ is similar to the central neutron channel [Fig. 2(b)], while the off-axis charge-exchange signal is predicted to be largest for intermediate $D$, since virtually no trapped beam ions reach $R = 2.97$ m for $D = 0$ [Fig. 2(c)].

The data fall between the $D = 0$ and the $D = 0.1$ m$^2$/sec predictions. The central measurements agree best with the $D = 0$ prediction [Figs. 2(a), 2(b), and 2(d)]. [The difference between the $D = 0$ prediction and experiment is within experimental error ($\sim 10\%$) and may be caused by a slight overestimate of the central density.] The off-axis signals require diffusion of order 0.1 m$^2$/sec to match the experiment [Figs. 2(c) and 2(f)]. Perhaps large-angle scattering, which is neglected in our Fokker–Planck calculations, increases energy diffusion (resulting in a slower central decay rate) and increases pitch-angle scattering (giving a larger off-axis charge-exchange signal). Alternatively, the true diffusion coefficient may increase with radius. In any event, the data indicate that the average beam-ion diffusion is less than 0.1 m$^2$/sec.

This conclusion is consistent with the data from other Ohmic discharge conditions with $I_p = 0.8$–$1.6$ MA, $B_T = 3.1$–$4.1$ T, $R_0 = 2.42$–$2.60$ m, and $\bar{n}_e = 0.7$–$2.0 \times 10^{19}$ m$^{-3}$ (Fig. 3). In particular, a plasma condition with a large $m = 4$, $n = 1$ nonrotating, ("locked") mode and one with an out-shifted magnetic axis (to enhance ripple losses) are included. Discharges where beam–beam reactions are calculated to predominate exhibit behavior similar to the discharges dominated by beam–target reactions. No systematic differences in fast-ion behavior between these conditions and the baseline condition (Fig. 2) are observed. Assuming that the same transport processes are operative in all of the discharges, the total neutron emission and central charge-exchange data indicate a central diffusion coefficient $D \ll 0.1$ m$^2$/sec [Figs. 3(a) and 3(b)], while the neutron profile and off-axis charge-exchange detector indicate $D \lesssim 0.1$ m$^2$/sec for $r/a \lesssim 0.5$ [Figs. 3(c) and 3(d)].

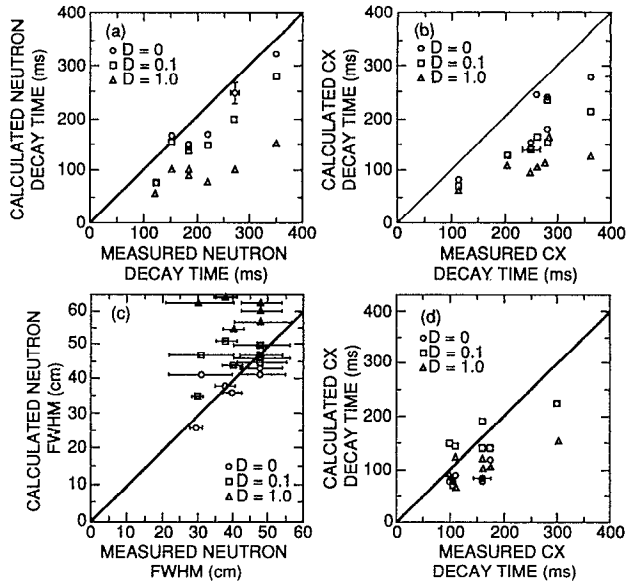


FIG. 3. Comparison of seven experimental conditions with theoretical simulations for $D = 0$, $D = 0.1$, and $D = 1.0$ m$^2$/sec. The lines indicate perfect agreement and the horizontal error bars are statistical uncertainties. (a) Time for the total neutron emission to decay one decade. The vertical error bar indicates the typical uncertainty associated with uncertainties in $T_e$ and $n_e$. (b) Time for the 50 keV, $R = 2.44$ m charge-exchange signal to decay one decade. (c) The width of the neutron profile when the total neutron emission has decayed one decade. (d) Time for the 50 keV, $R = 2.97$ m charge-exchange signal to decay one decade.

## III. DISCUSSION

Typical TFTR diffusion coefficients and thermal diffusivities[5,20] are $\sim 1.0$ m$^2$/sec. For example, in the discharge of Fig. 2, the electron thermal diffusivity at $r/a \simeq 0.3$ is approximately $\chi_e \gtrsim 0.5$ m$^2$/sec. This value is an order of magnitude larger than our bound on the beam-ion diffusion coefficient $D$. A likely explanation for the difference between thermal transport and fast-ion transport is that beam ions do not stay in resonance with the fluctuations responsible for thermal transport since their drift orbit displacements exceed the radial correlation length $\Delta_m$ of the fluctuations.[5,21] (A similar process may account for enhanced high-energy runaway electron confinement.[21]) If one assumes that this explanation is correct, then the observed ratio of $D/\chi_e$ implies that the fluctuations responsible for transport have a radial scale length significantly smaller than $\rho_f \sim 1$ cm. In contrast to the thermal transport (which is far in excess of neoclassical expectations), the central beam-ion diffusion coefficient is consistent with the diffusion predicted by neoclassical theory [$D \sim O(0.01$ m$^2$/sec)]. (The neoclassical pinch velocity is negligible.) The diffusion of off-axis banana-trapped ions does exceed the neoclassical prediction, however.

The sawtooth instability has been observed to transport fast ions.[22] For the condition documented in Fig. 2, the drop in central electron temperature at a sawtooth crash is only $\Delta T_e/T_e = 14\%$ and the inversion radius is only 0.13 m with an 18 msec period. Thus a relatively modest effect is expected. Another possible transport mechanism is associated with toroidal field ripple. The absence of perfect toroidal symmetry causes fast ions trapped in the $1/R$ field wells to suffer a small radial displacement at each poloidal half-orbit. For the plasma conditions of these experiments, either pitch-angle scattering or the finite radial excursions themselves are sufficient to decorrelate successive radial steps over most of the plasma, leading to radial diffusion. The expected "ripple-plateau" diffusivity[23] is strongly dependent on fast-ion energy ($D \propto E^{3/2}$) and on the magnitude of the toroidal field ripple. Since few beam ions are born on banana orbits (only neutrals ionized outside $R \simeq 3.05$ m are initially trapped), only the charge-exchange measurements are sensitive to ripple transport. For plasmas centered at $R = 2.42$ m, the calculated ripple transport is very small [e.g., $D(E = 90$ keV$) \simeq 0.01$ m$^2$/sec at $R = 2.5$ m, $z = 0.3$ m], which is consistent with the absence of observable diffusion in the central charge-exchange signal [Fig. 3(b)]. The expected ripple transport increases rapidly with increasing major radius. For example, at $R = 3.0$ m and $z = 0.3$ m the expected diffusion of 90 keV ions due to field ripple is $D(E = 90\,\text{keV}) \sim 1.0$ m$^2$/sec. In our simulations, the data from the charge-exchange detector at $R = 2.97$ m are consistent with a *spatially averaged* diffusion coefficient of $\sim 0.1$ m$^2$/sec [Fig. 3(d)]. Thus it seems likely that ripple transport affects the signal measured by this detector.

In conclusion, in low-beta TFTR plasmas ($\beta_t \lesssim 0.2\%$) with small beam-ion concentrations ($n_b/n_e \lesssim 10\%$) the deceleration rate of beam ions agrees well with classical theory, as it did in DIII-D.[1] The agreement of the volume-integrated neutron source strength with the simulations indicates that the central fast-ion diffusion coefficient is much less than 0.1 m$^2$/sec, which is much smaller than thermal transport coefficients. Thus a key assumption of conventional transport analysis (that beam-ion behavior is classical) is validated, as are the transport simulations of the initial beam deposition. It should be noted, however, that more intense beam populations could modify the fluctuation spectrum in a manner that increases fast-ion transport. Future work will investigate beam-ion transport during strong auxiliary heating. The difference between $D$ and $\chi_e$ suggests that microturbulence with decorrelation lengths smaller than 1 cm are responsible for thermal transport. Finally, the small beam-ion diffusion suggests that, in the absence of collective fast-ion driven instabilities, alphas in a reactor will thermalize more rapidly than they will be lost.

## ACKNOWLEDGMENTS

The contributions of the TFTR staff are gratefully acknowledged. W. W. H., C. W. B., and Y. K. thank Dale Meade and Ken Young for supporting their visits to TFTR.

This work was supported by U.S. Department of Energy Contract No. DE-AC02-76-CHO-3703.

[1] W. W. Heidbrink, J. Kim, and R. J. Groebner, Nucl. Fusion **28**, 1897 (1988); W. W. Heidbrink, Phys. Fluids B **2**, 4 (1990).
[2] M. Tuszewski and J. P. Roubin, Nucl. Fusion **28**, 499 (1988).
[3] A. Carnevali, S. D. Scott, H. Neilson, M. Galloway, P. Stevens, and C. E. Thomas, Nucl. Fusion **28**, 951 (1988).
[4] J. D. Strachan, P. L. Colestock, S. L. Davis, D. Eames, P. C. Efthimion, H. P. Eubank, R. J. Goldston, L. R. Grisham, R. J. Hawryluk, J. C. Hosea, J. Hovey, D. L. Jassby, D. W. Johnson, A. A. Mirin, G. Schilling, R. Stooksberry, L. D. Stewart, and H. H. Towner, Nucl. Fusion **21**, 67 (1981).
[5] P. C. Efthimion, M. Bitter, E. D. Fredrickson, R. J. Goldston, G. W. Hammett, K. W. Hill, H. Hsuan, R. A. Hulse, R. Kaita, D. K. Mansfield, D. C. McCune, K. M. McGuire, S. S. Medley, D. Mueller, A. T. Ramsey, S. D. Scott, B. C. Stratton, K.-L. Wong, H. Biglari, P. H. Diamond, Y. Takase, and V. A. Vershkov, in *Plasma Physics and Controlled Nuclear Fusion Research 1988* (IAEA, Vienna, 1989), Vol. 1, p. 307.
[6] P. C. Efthimion, N. Bretz, M. Bell, M. Bitter, W. R. Blanchard, F. Boody, D. Boyd, C. Bush, J. L. Cecchi, J. Coonrod, S. Davis, D. Dimock, H. F. Dylla, S. von Goeler, R. J. Goldston, B. Grek, D. J. Grove, R. J. Hawryluk, H. Hendel, K. W. Hill, R. Hulse, D. Johnson, L. C. Johnson, R. Kaita, S. Kaye, M. Kikuchi, S. Kilpatrick, J. Kiraly, R. Knize, P. LaMarche, R. Little, D. Manos, M. McCarthy, D. McCune, K. McGuire, D. M. Meade, S. S. Medley, D. R. Mikkelsen, D. Mueller, M. Murakami, E. B. Nieschmidt, D. K. Owens, A. T. Ramsey, A. L. Roquemore, N. R. Sauthoff, J. Schivell, J.-L. Schwob, S. Scott, S. Sesnic, J. Sinnis, F. Stauffer, J. D. Strachan, S. Suckewer, G. D. Tait, M. Tavernier, G. Taylor, F. Tenney, H. Towner, M. Ulrickson, K.-L. Wong, A. Wouters, H. Yamada, K. M. Young, and M. Zarnstorff, in *Plasma Physics and Controlled Nuclear Fusion Research 1984* (IAEA, Vienna, 1985), Vol. I, p. 29.
[7] David L. Book, *NRL Plasma Formulary* (Naval Research Laboratory, Washington, DC, 1990), p. 31.
[8] G. Taylor, P. Efthimion, M. McCarthy, V. Arunasalam, R. Bitzer, J. Bryer, R. Cutler, E. Fredd, M. A. Goldman, and D. Kaufman, Rev. Sci. Instrum. **55**, 1739 (1984).
[9] H. Park, Plasma Phys. Controlled Fusion **31** (1989) 2035; H. Park, Rev. Sci. Instrum. **61**, 2879 (1990).
[10] D. Johnson, N. Bretz, D. Dimock, B. Grek, D. Long, R. Palladino, and E. Tolnas, Rev. Sci. Instrum. **57**, 1856 (1986).
[11] A. T. Ramsey and S. L. Turner, Rev. Sci. Instrum. **58**, 1211 (1987).
[12] H. W. Hendel, R. W. Palladino, Cris W. Barnes, M. Diesso, J. S. Felt, D. L. Jassby, L. C. Johnson, L.-P. Ku, Q. P. Liu, R. W. Motley, H. B. Murphy, J. Murphy, E. B. Nieschmidt, J. A. Roberts, T. Saito, J. D. Strachan, R. J. Waszazak, and K. M. Young, Rev. Sci. Instrum. **61**, 1900 (1990).
[13] A. L. Roquemore, R. C. Chouinard, M. Diesso, R. Palladino, J. D. Strachan, and G. D. Tait, Rev. Sci. Instrum. **61**, 3163 (1990).
[14] J. D. Strachan, A. L. Roquemore, M. Diesso, S. L. Liew, and J. Roberts, *Proceedings of the 17th European Conference on Controlled Fusion and Plasma Heating* (North-Holland, Amsterdam, 1990), Vol. 14B, Part IV, p. 1548.
[15] C. W. Barnes, M. G. Bell, H. W. Hendel, D. L. Jassby, D. Mikkelsen, A. L. Roquemore, S. D. Scott, J. D. Strachan, and M. C. Zarnstorff, Rev. Sci. Instrum. **61**, 3151 (1990).
[16] R. Kaita, G. W. Hammett, G. Gammel, R. J. Goldston, S. S. Medley, S. D. Scott, and K. M. Young, Rev. Sci. Instrum. **59**, 1691 (1988).
[17] R. J. Goldston, D. C. McCune, H. H. Towner, S. L. Davis, R. J. Hawryluk, and G. L. Schmidt, J. Comput. Phys. **43**, 61 (1981); R. J. Hawryluk, in *Physics of Plasmas Close to Thermonuclear Conditions* (CEC, Brussels, 1980), Vol. 1, p. 19.
[18] R. J. Goldston, Nucl. Fusion **15**, 651 (1975).
[19] R. Budny and the TFTR Group, J. Nucl. Mater. **176-177**, 427 (1990).
[20] E. J. Synakowski, B. C. Stratton, P. C. Efthimion, R. J. Fonck, R. A. Hulse, D. W. Johnson, D. K. Mansfield, H. Park, S. D. Scott, and G. Taylor, Phys. Rev. Lett. **65**, 2255 (1990); P. C. Efthimion, D. K. Mansfield, B. C. Stratton, E. Synakowski, A. Bhattacharjee, H. Biglari, P. H. Diamond, R. J. Goldston, C. C. Hegna, D. McCune, G. Rewoldt, S. Scott, W. M. Tang, G. Taylor, R. E. Waltz, R. M. Wieland, and M. C. Zarnstorff, *ibid.* **66**, 42 (1991).
[21] H. E. Mynick and J. A. Krommes, Phys. Rev. Lett. **43**, 1506 (1979).
[22] G. Martin, O. N. Jarvis, J. Källne, V. Merlo, G. Sadler, and P. van Belle, Phys. Scr. **T16**, 171 (1987); J. A. Lovberg, W. W. Heidbrink, J. D. Strachan, and V. S. Zaveryaev, Phys. Fluids B **1**, 874 (1989) and references therein.
[23] R. J. Goldston and H. H. Towner, J. Plasma Phys. **26**, 283 (1981).